Heliyon 8 (2022) e09279

Contents lists available at ScienceDirect

Heliyon

journal homepage: www.cell.com/heliyon

Research article

A unique, inexpensive, and abundantly available adsorbent: composite of synthesized silver nanoparticles (AgNPs) and banana leaves powder (BLP)

Mona A. Darweesh [a], Mahmoud Y. Elgendy [b,*], Mohamed I. Ayad [b], Abdel Monem M. Ahmed [c], N.M. Kamel Elsayed [d], W.A. Hammad [a]

[a] Engineering Physics & Mathematics Department, Faculty of Engineering, Tanta University, Egypt
[b] Chemistry Department, Faculty of Science, Menoufia University, Egypt
[c] Chemistry Department, Faculty of Science, Alexandria University, Egypt
[d] Faculty of Pharmacy, Alexandria University, Egypt

HIGHLIGHTS

- By reduction reaction, silver nanoparticles were impregnated in banana leaves homogeneous powder and used as an adsorbent.
- The fabricated composites are used as adsorbent for the removal of Zn (II), Pb (II), and Fe (III) ions from aqueous solutions.
- The new adsorbent exhibited high adsorption capacity with three metal ions and followed the order Pb (II)> Fe (III) >Zn (II) ions.
- The metal ions vanished from the solution within approximately 40 min.

ARTICLE INFO

Keywords:
Agriculture waste
Banana leaves
Heavy metals
Ions removal
Silver nanoparticles
Adsorption kinetics
Adsorption isotherm

ABSTRACT

The purpose of this study is to investigate the development of a new and inexpensive adsorbent by immobilization synthesized silver nanoparticles (AgNPs) onto banana leaves powder (BLP), and the prepared composite (BLP)/(AgNPs) was used as an adsorbent for Zn(II), Pb(II), and Fe(III) ion removal from aqueous solutions under the influence of various reaction conditions. (BLP)/(AgNPs) demonstrated remarkable sensitivity toward Zn (II), Pb (II), and Fe (III) ions; metal ions eliminations increased with increasing contact time, agitation speed, adsorbent dose, and temperature, yielding adequate selectivity and ideal removal efficiency of 79%, 88%, and 91% for Zn (II), Pb (II), and Fe (III) ions, respectively, at pH = 5 for Zn(II) and pH = 6 for Pb(II), and Fe(III). The equilibrium contact time for elimination of Zn (II), Pb (II), and Fe (III) ions was reaches at 40 min. Langmuir, Freundlich, and Temkin equations were used to test the obtained experimental data. Langmuir isotherm model was found to be more accurate in representing the data of Zn(II), Pb(II), and Fe(III) ions adsorption onto (BLP)/(AgNPs), with a regression coefficient (R^2 = 0.999) and maximum adsorption capacities of 190, 244, and 228 mg/g for Zn(II), Pb(II), and Fe(III) ions, respectively. The thermodynamic parameters proved that adsorption of metal ions is spontaneous, feasible, and endothermic, whereas Kinetic studies revealed that the process was best described by a pseudo second order kinetics.

1. Introduction

Clean water is the aspiration and basic requirement of people all over the world. Clean, safe water resources are in short supply and this crisis is caused by the rapid growth of the world population, global warming, and the natural, rapid decline of water resources. Therefore, the economical use of water resources, the use of treated wastewater for agriculture and industry, and the use of low-cost and environmentally friendly technologies are effective ways to conserve limited freshwater resources and successfully contribute to the world's clean water [1, 2]. Heavy metals' presence in water resources is a global problem, as most of them are toxic to organisms, are not biodegradable, and tend to accumulate in biota, compromise the immune system, cause cancer, and threaten life on earth [3]. The coexistence of pollutants such as heavy metals in water sources may be due to common geological sources or increased wastewater discharge from different industries, such as: metallurgical, tanning,

* Corresponding author.
E-mail address: ma7moudelgendy@yahoo.com (M.Y. Elgendy).

https://doi.org/10.1016/j.heliyon.2022.e09279
Received 4 December 2021; Received in revised form 8 January 2022; Accepted 11 April 2022

plating, mining, fertilizer, metal finishing, welding alloy manufacturing plants, fertilizers, chemicals, etc. [4, 5]. Trivalent, and divalent heavy metal ions such as, Fe^{+3},Zn^{+2} and Pb^{+2}, are irreplaceable in all walks of life, and even small concentrations can pose a serious threat to human health since they can be effective in the food chain and may threaten all forms of life [6]. The high threat of heavy metal ions propels researchers to look for changed strategies to safeguard the environment and individuals through different remediation processes [7]. Traditional methods similar to chemical precipitation, reduction, solvent extraction, electrochemical deposition, electrolysis, filtration, and ion exchange have been used, but the majority of these methods are either economically unsuitable or inefficient, particularly for a lower concentration of heavy metal ions [8]. The adsorption method is one of the most widely used ideals, productive, and cost-effective methods for purifying water and wastewater [9, 10]. Different adsorbents such as clays, agriculture waste, carbon nanotubes, silica, polymers, and activated carbons have been studied to purify wastewater from heavy metal ions [11, 12, 13]. Adsorbents derived from agriculture waste are regarded as widely abundant, environmentally friendly, and fitting for varied environmental conditions due to their efficiency over wide pH ranges, but slow adsorption and feeble affinity for heavy metals motivate researchers to investigate chemical modification of agriculture waste adsorbents [14]. Some crops are common and grown all year round, such as bananas which are grown in more than 130 countries in the world, and the world production of bananas every year is estimated by millions tons [15]; Therefore, banana agricultural waste may be a source of adsorbents, and the extracted sieved banana leaves homogeneous powder (BLP) can be used as adsorbents to purify wastewater. Nanomaterials have been used as adsorbents in wastewater treatment and have received considerable attention because of their higher efficiency and lower cost compared to ancient materials [16]. The high surface area, high surface free energy, and great density of active sites per unit mass, result in enhanced surface reactivity of nanomaterials, making them good adsorbents [17, 18]. Due to their favorable chemical and physical properties, silver nanoparticles (AgNPs) have been investigated as suitable adsorbents due to their good performance, their high surface area, high catalytic activity, excellent biocompatibility, relatively low cost, and high adsorption capacity [19, 20]. There are different studies in the literature using silver nanoparticle composites as adsorbents to eliminate heavy metal ions and organic pollutants in aqueous solutions, showing good applicability and high efficiency [21, 22]. But, the applicability of NPs in wastewater purification may be restricted due to their low stability and tendency to aggregate [2]. Therefore, mechanical support such as banana leaves powder (BLP) is used to hold AgNPs for possible applications in wastewater treatment. (BLP) is considered an abundant and environmentally friendly agricultural waste that can be used as an adsorbent [14]. To maximize the adsorption efficiency, take advantage of both (BLP) and (AgNPs), overcome AgNPs aggregation and avoid release into solution, silver ions were impregnated into the (BLP) by taking advantage of their inherent porosity, followed by reduction of silver ions into silver nanoparticles. (BLP) was used to hold (AgNPs) because of its high oxygen density, which acts as a binding site for AgNPs [23]. The objective of this work is to fabricate (BLP)/(AgNPs) composite with the advantages of both (BLP) and (AgNPs) for removing Fe (III), Pb (II), and Zn (II) from aqueous solutions. Several reaction conditions that influence heavy metal ion uptake were investigated, including initial metal ion concentration, adsorbent dose, temperature, agitation speed, and solution pH.

2. Experimental

2.1. Materials

Silver nitrate was supplied by GAMMA laboratory chemicals. Glucose was purchased from El-Nasr Chemicals Co. (ADWIC, Egypt). Anhydrous ferric sulfate, Lead nitrate, and Zinc Nitrate Hexahydrate were purchased from Research-Lab Fine Chemical industries. All chemicals were of high grade quality, and all solutions were prepared in demineralized water following the standard procedures.

2.2. Preparation of metal solution

The stock solutions of Zn(II), Pb (II), and Fe (III) were prepared by dissolving the desired amount of metal salts in double-distilled water. The working solutions (50–250 mg/L) of the examined metal ions were adjusted by appropriate dilution of the stock solutions with double-distilled water.

2.3. Banana leaves powder preparation

The collected banana leaves were washed with hot distilled water to separate the impurities, and dried for 24 h, before being used as mechanical support to hold AgNPs in the reduction reaction.

2.4. Synthesis of silver nanoparticles impregnated in banana leaves powder

Silver nanoparticles (AgNPs) were trapped on the given banana leaves powder via reductions of Ag^{+} ions in aqueous solution. In a reaction mixture, 1 g of BLP was soaked with 50 ml of water, stirred with $AgNO_3$, and followed by the addition of glucose solution. The total volume of reaction mixture was 100 ml. The concentration of $AgNO_3$ was in the range of 0.005–0.07 mol/L, while the glucose concentration was 0.05 mol/L. The mixture was then stirred for 45 min at 75 °C. The surface of BLP appeared coated with a dark brown precipitate, referring to the formation of AgNPs. The resultant material was filtered, washed with distilled water, and dried at 60 °C for 2 h. The generation of AgNPs was assured by obtaining the absorbance of the reaction mixture filtrate spectrophotometrically at λ_{max} = 420 nm. The intense band that appeared around 420 nm is indicated to be a surface plasmon resonance band that appeared due to the excitation of the free electrons in AgNPs [22].

2.5. Characterization techniques

The crystalline phases were determined using X-ray diffraction (XRD, GNR APD-2000 PRO X-ray). Infrared transmittance measurements of (BLP) and (BLP)/(AgNPs) were performed on a PerkinElmer 1430 spectrometer using KBr pellets. The morphology of BLP/AgNPs was examined using a scanning electron microscope (SEM), Joel-JSM-6510 TV.

2.6. Adsorption measurements

Batch adsorption experiments were used for the removal of Zn (II), Pb (II), and Fe (III) from synthetic solutions by (BLP)/(AgNPs) composite. A digital magnetic stirrer MS-H-Pro with a temperature sensor PT 1000 and a Teflon coated magnetic stir bar of 2 cm length is used to stir the heavy metal ion solution with (BLP)/(AgNPs) composite. A predetermined volume of heavy metal ions solution with a predetermined initial concentration is stirred with a predetermined amount of (BLP)/(AgNPs) composite for a predetermined time at a fixed agitation rate, temperature, and pH of the solution, which was modified by the addition of NaOH (0.1 mol/L) or HCl (0.1 mol/L) and measured using a digital pH meter (Model pH System-361, India). For one analysis, 1 ml samples were taken at regular intervals and filtered out of the (BLP)/(AgNPs)/heavy metal ions solution chemical reaction. The atomic absorption spectrophotometer, AAS, (Model, AA55; Varian Inc., USA), was used to measure the concentration of heavy metal ions in the filtrate. The amount of heavy metal ions adsorbed per unit mass of adsorbent (mg/g) at time t, (q_t) was determined by Eq. (1) and the removal percentage (R %) was determined by Eq. (2),

$$q_e = (C_o - C_e)\frac{V}{m} \quad (1)$$

$$R(\%) = \frac{(Co - Ct)}{Co} \times 100 \quad (2)$$

where, the initial concentration of heavy metal ions represented by C_o, C_t determines the heavy metal ions concentration at time t (mg/l), V is the solution volume (L), and m is the mass per gram of adsorbent.

3. Results and discussion

3.1. Characterization

3.1.1. X-ray diffraction pattern

XRD is characterized as a good fingerprint fitting characterization technique, which is used to explore phase and crystal structure [24]. The results of the X-ray are shown in (Figure 1). The detected peak for BLP is due to the cellulose group crystal plane [25]. The values obtained for the intense peak at 22.55 are attributed to the presence of native cellulose as the prime component, which may be crystalline or amorphous [26]. The new composite produced from (AgNPs) impregnated (BLP) can be crystallographically characterized by peaks of AgNPs around 2θ = 38.2, 45.15, and 64.36, characterize the diffraction planes of (1 1 1), (2 0 0), and (2 2 0) respectively, which relate to the face centered cubic crystal structure of silver, Generally, the broad and small peaks in the X-ray diffraction pattern are related to the small particle size, and the peaks of AgNPs around 2θ = 45.15, and 64.36, suggest that the smaller AgNPs are embedded in the BLP. This obviously confirms the fabrication of stable Ag nanoparticles on BLP [27].

3.1.2. FT-IR spectra

The FTIR spectroscopy was used to identify the functional groups of (BLP) and to prove that silver nanoparticles are formed. It helps in studying the chemical composition of fabricated (BLP)/(AgNPs) composites, hence feasible interactions between its functional groups with heavy metal ions [28]. The FT-IR spectra of (BLP) and (BLP)/(AgNPs) are shown in Figure 2 As indicated, the strong adsorption peaks at 3420.54 cm^{-1} confirms the presence of O–H stretch (alcohol, phenol, carboxylic acid) group [29]. The peaks observed at 2920.39 cm^{-1} and 2852 cm^{-1} are assigned to asymmetric C–H and symmetric C–H groups stretching [30]. The peaks at 1732.58 cm^{-1} are characteristics of the bending of the C=O group [31]. The peak at 1518.25 cm^{-1} was assigned to C=C

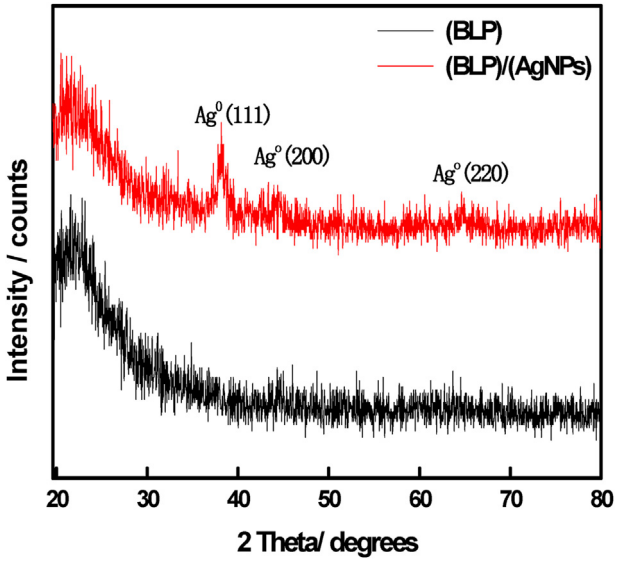

Figure 1. XRD spectra of BLP and (BLP)/(AgNPs) composite.

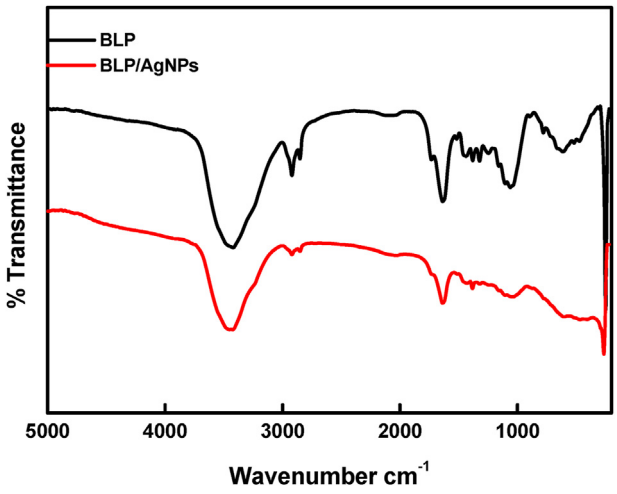

Figure 2. FTIR spectra of BLP and BLP/AgNPs composite.

stretching vibration of the aromatic ring, and that at 1380.73 cm^{-1} was assigned to Aliphatic C–H stretching in CH_3,C–O stretching, CH bending [32]. The band at 1322.59 cm^{-1} represented C–C and C–O ring stretching vibrations [33], whereas those at 1246.23 cm^{-1} could be assigned to the C–C, C–O and C=O stretching [34]. In addition, the peaks at 897 cm^{-1} and 665 cm^{-1} are attributed to the C–H rocking vibrations of cellulose and C–O–H group,respectively [33, 34, 35]. Thus, the disappearance of some peaks, and shifts in the intensity of some bands, after impregnation with AgNPs indicate that AgNPs were successfully loaded onto the (BLP). The presence of these functional groups can facilitate the adsorption of heavy metal ions.

3.1.3. Morphology of composite

The SEM image characterization is technique used to obtain the surface morphology of the created adsorbent (BLP/AgNPs). As shown in Figure 3, it is clear that the AgNPs (white spots) have a semispherical form and a uniform size distribution. Due to the strong affinity of silver for oxygen and nitrogen in the functional group of BLP, AgNPs were well adhered to the BLP surface [22].

3.2. Adsorption of heavy metal ions and effect of reaction parameters

The adsorption experiments were conducted by examining the (BLP)/(AgNPs) composite for Zn (II), Pb(II), and Fe(III) ions elimination from aqueous solutions. The adsorption process was carried out by varying contact time, initial heavy metal ion concentration, temperature, adsorbents dose, agitation speed, and pH of the solution. The specific effect of each parameter is examined and methodically studied. The experimental findings demonstrated the expected sensitivity to Zn (II), Pb (II), and Fe

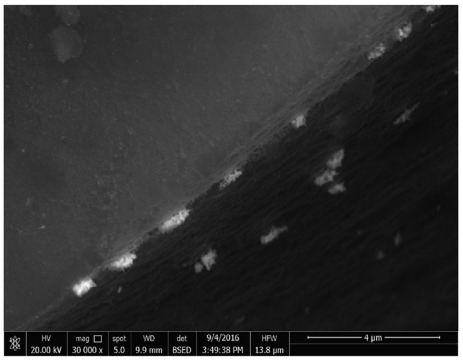

Figure 3. SEM image of BLP/AgNPs composite.

(III) ions in aqueous solutions and exhibited priority for each metal ion at a particular pH. The following optimum experimental conditions: adsorbent mass of 0.1 g, metal ion concentration of 100 ppm, agitation speed of 300 rpm, and 0.1 L of aqueous solutions at 30 °C, pH = 5, for Zn (II), and pH = 6 for Pb (II) and Fe (III) ions, were adjusted barring otherwise specified.

3.2.1. Effect of contact time

The effect of contact time on (50–250) ppm of Zn (II), Pb (II), and Fe (III) ions adsorption onto BLP/AgNPs was studied, while all other variables were kept constant. Figure 4 indicates the effect of contact time on the removal percentage of initial concentration of 50 ppm of Zn (II), Pb (II), and Fe (III). The removal percentage of Zn (II), Pb (II), and Fe (III) ions removed at time t, increased sharply over time and reached a stage of stability after ~35 min. Almost 70%, 70%, and 75% of Zn (II), Pb (II), and Fe(III) ions, respectively removed with 35 min of stirring. Increasing the contact time raises the metal ions uptake efficiency. The equilibrium contact time for Zn (II), Pb (II), and Fe(III) ions removal was estimated by 35 min, because of the sorption efficiency is approximately close to 35 min contacted time as increasing contact time up to 120 min. The adsorption of Zn (II), Pb (II), and Fe (III) ions onto the BLP/AgNPs adsorbent mainly follows the intraparticle diffusion model and adsorption complexation mechanisms [36]. The percentage of Zn (II), Pb (II), and Fe(III) ions adsorption increased rapidly during the initial stage, This is because the active sites on the (BLP)/(AgNPs) surface were available. Subsequently, the adsorption of heavy metal ions decreased as the availability of the vacant sites for adsorption reduced over time.

3.2.2. Adsorbent dose effect

The adsorption efficiency of the batch adsorption process is substantially governed by the quantity of adsorbent dose and adsorbent/solution ratio [37]. The removal percentages of Zn (II), Pb (II), and Fe(III) ions were obtained at different doses of BLP/AgNPs and fixed metal ions concentrations. As shown in Figure 5 the removal percentage increased from (73–95%), (84–100%), and (86–100%) for Zn (II), Pb (II), and Fe (III) ions, respectively, by increasing the amount of BLP/AgNPs dose from 0.05 to 0.25 g. This behavior may be due to the fact that, the higher quantity of adsorbent dose in adsorption process, the greater surface area, hence available exchangeable sites for the ions [38].

3.2.3. The effect of initial Zn (II), Pb (II), and Fe (III) ion concentrations

In order to examine the effect of the initial concentration of Zn (II), Pb (II), and Fe (III) ions on adsorption reactions, the metal ion concentration was varied in the range of 50–250 ppm with a fixed dose (0.1) g of BLP/AgNPs. Figure 6 shows that, the removal percentage of Zn (II), Pb (II), and Fe (III) ions decreases with increasing the initial concentration from (84–60%), (90–73.6%) and (98–76%), respectively, as the metal ions

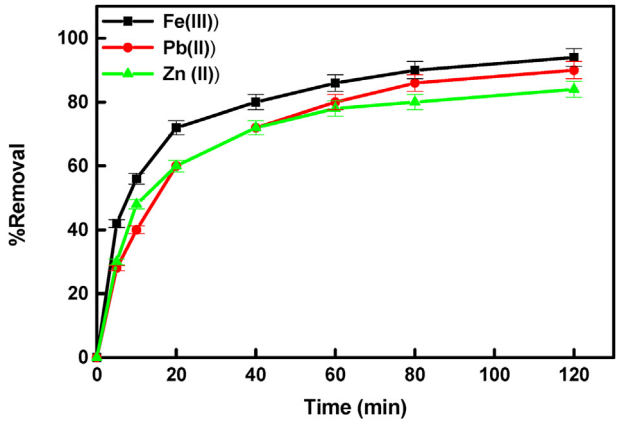

Figure 4. Effect of contact time on the removal percentage of (50 ppm) Zn (II), Pb (II), and Fe (III) ions on BLP/AgNPs.

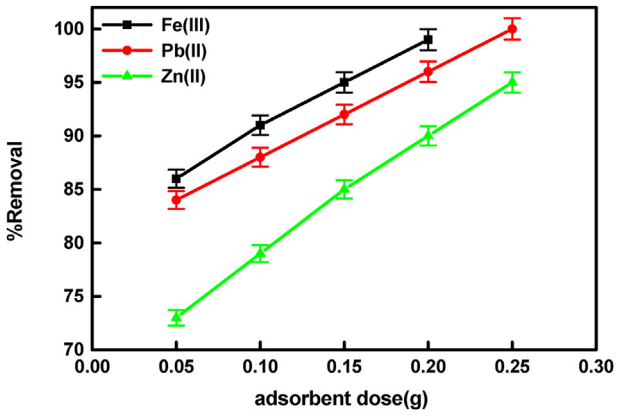

Figure 5. Effect of adsorbent dose on the removal percentage of Zn (II), Pb (II), and Fe (III) ions.

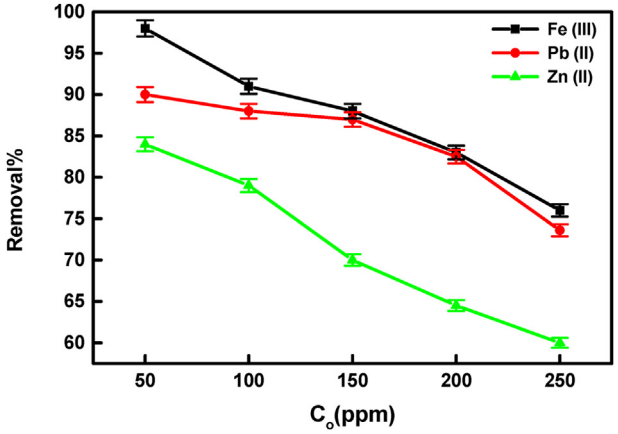

Figure 6. Effect of metal ions' concentration on the removal percentage of Zn (II), Pb (II), and Fe (III) ions.

concentration increases from 50 to 250 ppm. The percentage of removal depended upon the initial metal ions concentration may be due to the presence of abundant active sorption sites on the BLP/AgNPs surface at low concentrations of metal ions, and free BLP/AgNPs surface of metal ions, but at high concentrations, a few active sites on the BLP/AgNPs surface hinder the adsorption of more metal ions present in the solution [39].

3.2.4. The influence of temperature

The experimental results confirmed the great effect of temperature on the adsorption capacity of BLP/AgNPs, and Zn (II), Pb (II), and Fe (III) ions removed from aqueous solutions. The adsorption experiments were conducted at defined temperatures in the range of 25 °C–40 °C Figure 7 depicts an increase in the percentage of Zn(II), Pb(II), and Fe(III) ions removed by (BLP/AgNPs) from (70–86%), (82–96%), and (82–95%), respectively, as temperature increases from 25 to 40 °C). This improvement in Zn(II), Pb(II), and Fe(III) ion removal with high temperature could be attributed to an increase in the sorbate diffusion rate within the pores of the sorbent, as well as a reduction in liquid viscosity [40]. This reaction behavior confirms the endothermic nature of the adsorption process.

3.2.4.1. Thermodynamic parameters. Thermodynamic behavior of Zn (II), Pb (II), and Fe (III) ions adsorption onto (BLP/AgNPs) surface and the changes in the energies can be described via parameters such as the change in Gibbs free energy (ΔG°), enthalpy change (ΔH°) and entropy change (ΔS°) which were determined by Eq. (3),

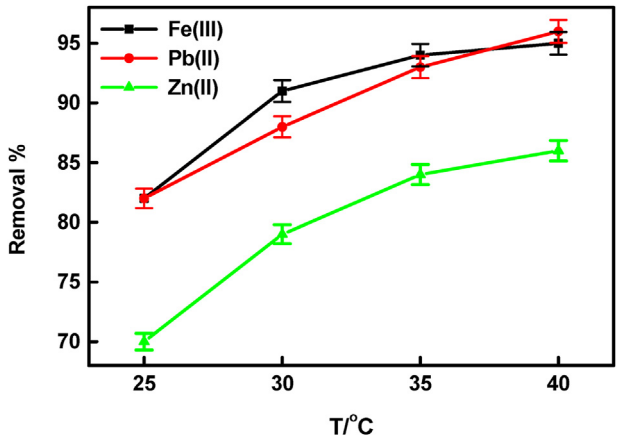

Figure 7. Influence of temperature on the removal percentage of Zn (II), Pb (II), and Fe (III) ions.

$$\Delta G^{\circ} = -RTLnK_C \quad (3)$$

where K_c represents the distribution coefficient of the solute, which is equal to q_e/C_e, R is the gas constant (8.314 J/mol K). The K_c values are used in Eq. (3) determine (ΔG°), (ΔH°) and (ΔS°) by Eq. (4).

$$\Delta G^{\circ} = \Delta H^{\circ} - T\,\Delta S^{\circ} \quad (4)$$

The values of other thermodynamic parameters may be obtained from the Van't Hoff equation, which is given by Eq. (5),

$$\ln K_C = \frac{\Delta S^{\circ}}{R} - \frac{\Delta H^{\circ}}{RT} \quad (5)$$

Thermodynamic parameters were extracted from van't Hoff linear plots ($\ln K_c$ vs 1/T) by determining the slope and intercept (Figure 8). According to results tabulated in Table 1, the positive values of ΔH° refer to endothermic adsorption of Zn(II), Pb(II), and Fe(III) ions onto (BLP/AgNPs), The positive values of ΔS° propose increased randomness at the solid/solution interface. The spontaneity and feasibility of Zn (II), Pb (II), and Fe (III) ions adsorption were confirmed by the negative values of ΔG° [41].

3.2.5. The influence of agitation speed

Agitation speed of the reaction mixture is an intrinsic factor that influences the adsorption process by affecting the dispersion of the reactants, adsorbent/adsorbate rapprochement, and mass transfer. Figure 9 exhibits experimental results for the effect of agitation speeds of (100, 200, 300, and 400) rpm, on the adsorption of Zn(II), Pb(II), and Fe(III) ions onto the BLP/AgNPs surface, at constant other parameters. The removal efficiency increased from (63–82 %), (76–92 %) and from (80–94 %) for Zn(II), Pb(II), and Fe(III), respectively, as the agitation speed increased. The increase in removal percentage may be due to an increase in the diffusion rate of Zn(II), Pb(II), and Fe(III) ions in the bulk solution, decrease of the boundary layer, and increases the transfer rate of the ions in solution [42], whereas the slow agitation speed may cause adsorbent particle aggregation in the solution.

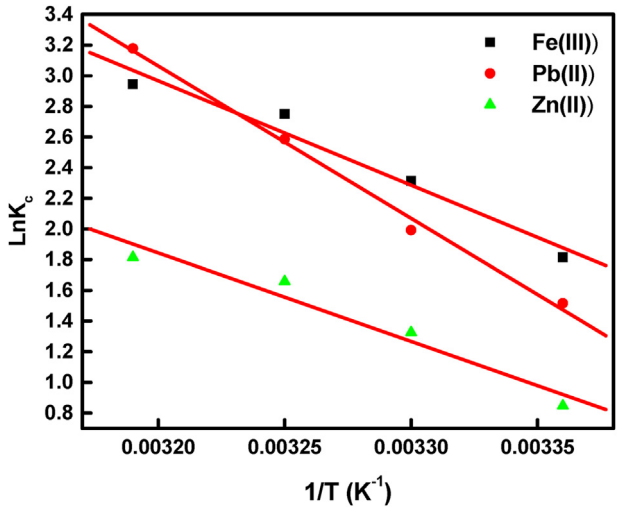

Figure 8. Plot of ln K_c and 1/T at the temperature range under consideration.

Table 1. Thermodynamic parameters of Zn (II), Pb (II), and Fe (III) ions adsorption onto the (BLP/AgNPs) surface.

Metal ion	ΔH° ($Jmol^{-1}$)	ΔS° ($Jmol^{-1}K^{-1}$)	ΔG° ($J.mol^{-1}$)			
			Temperature (K)			
			298	303	308	313
Zn(II)	694	2.44	-2099.2	-3337.6	-4246.2	-4723.9
Pb(II)	1195.9	4.1	-3756.8	-5019.2	-6623.7	-8270.2
Fe(III)	819	2.97	-4497.5	-5828.3	-7045.9	-7662.2

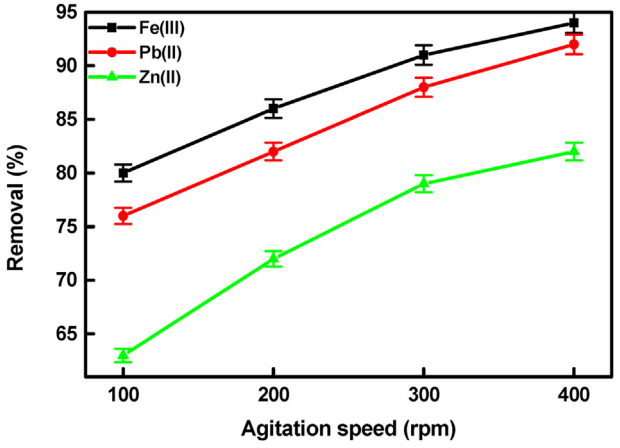

Figure 9. Agitation speed effect on the removal percentage of Zn(II), Pb(II), and Fe(III) ions.

3.2.6. The influence of solution pH

The solution pH has a great influence on the adsorption of heavy metal ions by affecting the solution chemistry of the heavy metals and the surface charge density of the adsorbent [43]. The effect of pH on the removal of Zn (II), Pb (II), and Fe (III) ions by the BLP/AgNPs composite was investigated, and the results are shown in Figure 10. The adsorption process was investigated at pH < 7 because, at higher pH values, heavy metal ions started to form insoluble metal hydroxides, which restricts true adsorption studies [44]. Figure 10 shows that for Zn (II), Pb (II), and Fe (III) ions, the removal percentage increased as a function of pH from (27–77%), (23–88%), and (30–91%), respectively. With Zn (II), Pb (II), and Fe (III) ions, removal percentages reached maximum values of 79% at pH (5), 88%, and 91% at pH (6), respectively. At low pH, the low adsorption and removal efficiency of Zn(II), Pb(II), and Fe(III) ions could be attributed to the competition of the binding sites on BLP/AgNPs surface for hydrogen ions, so metal ions cannot easily bond to the adsorbent surface [45]. In contrast, the removal percentage increases as pH increases due to the decrease in competition between protons (H^+) and positively charged metal ions at the surface sites. The BLP/AgNPs adsorbent is expected to have high adsorption efficiency at neutral or higher pH values, but precipitation of heavy metal ions as insoluble metal

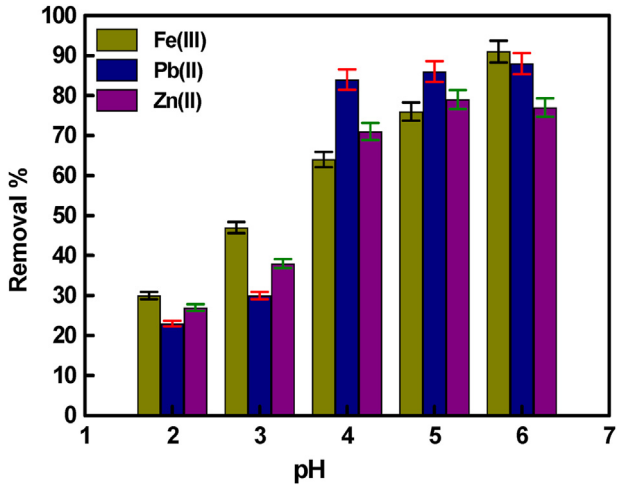

Figure 10. Effect of pH on the removal percentage of Zn(II), Pb(II), and Fe(III) ions.

hydroxides above pH 6 limits true evaluation of the adsorption process [46]. The metal ions may be bind strongly to the functional groups on the BLP/AgNPs surface with high stability via complexation formation. According to the experimental findings, the present adsorbents exhibited high Zn (II), Pb (II), and Fe (III) ions removal efficiency, and high adsorption capacities in regard to agricultural waste-based adsorbents.

3.3. Adsorption isotherms

The adsorption isotherms models are used to determine the mechanism of the adsorption process and indicate the distribution of adsorbate between solution and adsorbent at equilibrium [47]. The data obtained from adsorption of Zn (II), Pb (II), and Fe (III) ions onto BLP/AgNPs were analyzed using three isotherm models: Langmuir, Freundlich, and Temkin. The Langmuir adsorption isotherm assumes adsorption of homogeneous and monolayer surfaces. Eq. (6) defines the Langmuir adsorption isotherm,

$$\frac{C_e}{q_e} = \frac{1}{K_L\ q_m} + \frac{C_e}{q_m} \tag{6}$$

Where C_e is the concentration of the metal in solution at equilibrium (mg/L), q_e is a capacity of adsorption process at equilibrium (mg/g), q_m is a maximum capacity of active site (mg/g), and K_L (L mg^{-1}) is the Langmuir constant to determine the energy of adsorption. By drawing relation of C_e/q_e against C_e as shown in Figure 11, the values of q_m and K_L can be calculated from the slope and intercept of the plots, respectively,

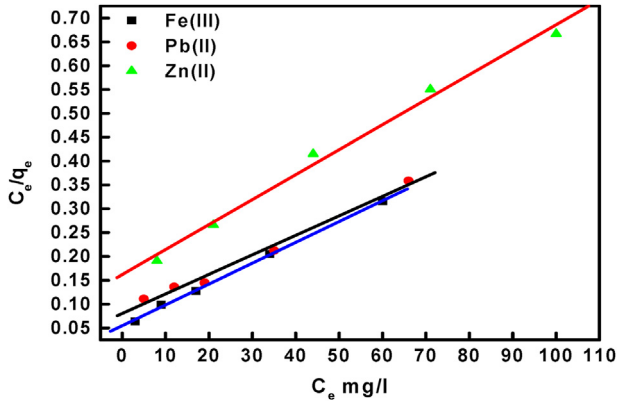

Figure 11. The Langmuir isotherm for Zn (II), Pb (II), and Fe (III) ions adsorption onto BLP/AgNPs surface.

and summarized in Table 2. In Langmuir isotherm model the affinity between the adsorbent and adsorbate were indicated via dimensionless separation factor (R_L) which is given by Eq. (7);

$$R_L = \frac{1}{1 + K_L C_\circ} \tag{7}$$

C_o represents initial metal ion concentration (mg/L). The characteristics of the R_L value indicate the nature of adsorption as favorable when its values lie between zero and one. The values of R_L calculated for Zn(II), Pb(II), and Fe(III) ions adsorption onto BLP/AgNPs are respectively 0.38, 0.28 and 0.2 at 50 mg L^{-1}, which indicate a favorable adsorption reactions. The empirical Freundlich equation is based on multilayer adsorption and a heterogeneous surface. The linear form of the Freundlich isotherm can be defined by Eq. (8).

$$\ln q_e = \ln K_F + \left(\frac{1}{n}\right)\ln C_e \tag{8}$$

where K_F and n are respectively determine the adsorption capacity and the adsorption intensity, and were determined from the intercept and slope of the plot of $\ln q_e$ versus $\ln C_e$, as shown in Figure 12. The resulted 1/n values which given in Table 2, confirm a great adsorption capacity of BLP/AgNPs. Temkin isotherm assumes a uniform distribution of binding energies and contains a factor that considers the heat of adsorbent interactions [48]. The model is given in linear form by Eq. (9),

$$q_e = B_t \ln A + B_t \ln C_e \tag{9}$$

where $B_t = RT/b$, b is corresponding to the heat of sorption (J/mol), and A is the equilibrium constant related to the maximum binding energy (l/g), T and R, are respectively, the absolute temperature (K) and gas constant (8.314 J/mol K), A graph of q_e against $\ln C_e$ are shown in (Figure 13) and the values of isotherm constants were determined and listed in Table 2. According to the adsorption constants obtained in Table 2, The Langmuir isotherm was found to be the most suitable model to describe the Zn(II), Pb(II), and Fe(III) ions adsorption onto BLP/AgNPs surface with correlation coefficient values is almost unity. The Langmuir isotherm agreement with the experimental findings, suggest a homogeneous surface and monolayer coverage. For evaluation of BLP/AgNPs as an adsorbent, the adsorption capacity of the BLP/AgNPs was compared with that of other previously studied adsorbents and listed in Table 3. Some previous studies discussed the employment of banana leaves, as adsorbent and exhibited moderate adsorption capacity [49], so there was an urgent need to improve the adsorption capacity of cheap and abundantly available adsorbents (banana leaves). This paper studied the modification of banana leaves surfaces by AgNPs to improve adsorption capacity. The new adsorbent BLP/AgNPs composite is employed to remove all coexisting metal ions and impurities, and will be an accurate relevant adsorbent for various effluents and wastewater.

Table 2. Isotherms data for adsorption of Zn(II), Pb(II), and Fe(III) ions onto BLP/AgNPs surface.

Adsorption isotherm	Parameters	Values for metal ions		
		Zn(II)	Pb(II)	Fe(III)
Langmuir	K_L	0.032 l g^{-1}	0.05 l g^{-1}	0.08 l g^{-1}
	q_m	190 mg g^{-1}	244 mg g^{-1}	228 mg g^{-1}
	R^2	0.995	0.993	0.999
Freundlich	K_F	16.2 mol g^{-1}	21 mol g^{-1}	30.5 mol g^{-1}
	1/n	0.49	0.55	0.47
	R^2	0.97	0.96	0.98
Temkin	Bt	41.7 J mol^{-1}	58 J mol^{-1}	49 J mol^{-1}
	A	0.324 l g^{-1}	0.81 l g^{-1}	0.81 l g^{-1}
	R^2	0.99	0.99	0.99

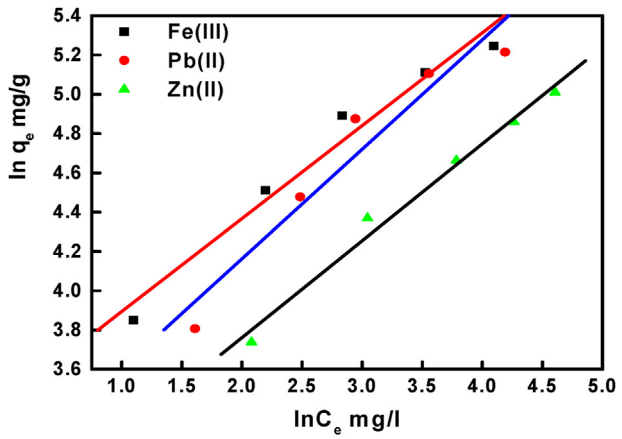

Figure 12. The Freundlich isotherm for Zn (II), Pb (II), and Fe (III) ions adsorption onto BLP/AgNPs surface.

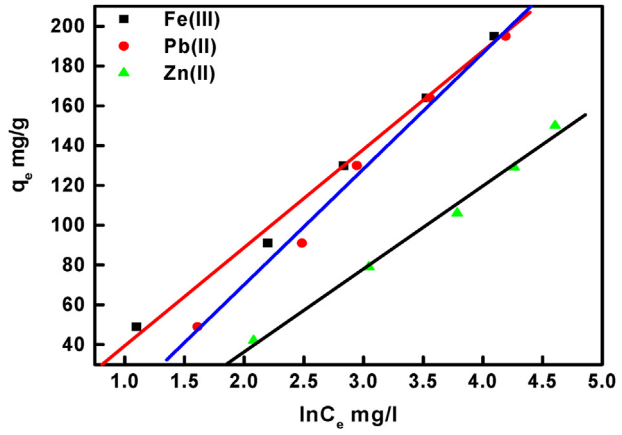

Figure 13. The Temkin isotherm for Zn (II), Pb (II), and Fe (III) ions adsorption onto BLP/AgNPs surface.

Table 3. Adsorption capacities of BLP/AgNPs composite for Zn (II), Pb (II), and Fe (III) ions compared to other previously studied adsorbents.

Adsorbents	q_m (mg/g) for metal ions as adsorbate			Reference
	Zn(II)	Pb(II)	Fe(III)	
BLP/AgNPs composite	190	244	228	This study
flax fibres	8.453	10.741		[50]
Albizia lebbeck pods	8.26	7.17		[51]
manganese dioxide-modified green biochar	22.38		70.67	[52]
bael leaves		125		[53]
tannic acid immobilised activated carbon	1.8		2.8	[54]

3.4. Adsorption kinetics

To further understand the adsorption behaviors; whether chemical reaction or mass transfer, and describe the metal ions' uptake, several kinetic models were used to model the rate of adsorption of Zn (II), Pb (II), and Fe (III) ions adsorption onto the BLP/AgNPs surface.

3.4.1. Pseudo-first-order kinetic model

This model describes the adsorption rate based on adsorption capacity, where it assumes that the heavy metal ions removal rates are associate with the quantity of the vacant adsorptive sites [55]. Eq. (10) is a general expression for the first-order Lagergren model.

$$\log(q_e - q_t) = \log q_e - \left(\frac{k_1}{2.303}\right)t \tag{10}$$

Where q_e and q_t are, respectively, the amounts of heavy metal ions adsorbed onto the BLP/AgNPs surface (mg/g) at equilibrium and at time t (min). The slope and intercept of plotting $\log(q_e - q_t)$ vs t, (not shown) are used to determine the Pseudo-first-order kinetic constant k_1 (1/min) and the equilibrium capacity q_e, respectively. The resultant values of q_e, k_1, and R^2 are tabulated in Table 4. The calculated values of q_e were greatly different from the experimental values, which suggest that, the adsorption of Zn (II), Pb (II), and Fe (III) ions onto BLP/AgNPs is not compatible with the Pseudo-first-order kinetic model.

3.4.2. Pseudo-second-order kinetic model

Pseudo-second-order reaction measures the metal ions adsorbed at time t and that adsorbed at equilibrium on the adsorbent surface [56, 57]. It is represented by Eq. (11);

$$\frac{t}{q_t} = \frac{1}{k_2\ q_e^2} + \frac{t}{q_e} \tag{11}$$

The t/q_t versus t plots (not shown) are used to determine parameters such as k_2, q_e, and R^2. Calculated values of the second-order rate constant k_2 (g mol^{-1} min^{-1}), and q_e (mg/g) were respectively extracted from the intercept and slope of the plot and presented in Table 4. The initial adsorption rate (h) was determined by calculated values of k_2 and q_e and defined by Eq. (12),

$$h = k_2 q_e^2 \tag{12}$$

The high correlation coefficient close to unity, $R^2 = 0.999$ and the satisfactory fitting of kinetic data in the second-order-model with obtained experimental results shows the compatibility of this model with the Zn(II), Pb(II), and Fe(III) ions adsorption onto the BLP/AgNPs surface, as shown in Table 4.

3.4.3. Intraparticle diffusion model

The previous pseudo-second-order models were unfitted to determine the diffusion mechanism, Weber and Morris developed Intraparticle diffusion model to study the steps of the diffusion mechanism, and investigate the nature of the rate-determining step [58]. The intra-particle diffusion is given by Eq. (13),

$$q_t = k_p t^{0.5} + C \tag{13}$$

where q_t (mg g^{-1}) is the amount of metal ions (Zn(II), Pb(II), and Fe(III)) adsorbed onto the adsorbents (BLP/AgNPs) at time t, K_p (mg/g $min^{0.5}$) is the intraparticle rate constants and C indicates to the boundary layer thickness caused by Zn(II), Pb(II), and Fe(III) adsorption onto BLP/AgNPs. The intraparticle diffusion plot (not shown), confirm that the adsorption process passes through two different stages. The first linear segment describes the external surface adsorption. The second linear segment describes the second stage in which the Zn (II), Pb (II), and Fe (III) ions are gradually adsorbed within the pores of BLP/AgNPs particles The rate constants of the two stages k_{p1} and k_{p2} are presented in Table 5, Additionally, the plot exhibited deviation from the origin which refers to that the intraparticle diffusion is not the only rate-limiting step and Zn(II), Pb(II), and Fe(III) ions adsorption process may be controlled by other kinetic models [59, 60].

3.4.4. Reaction mechanism

The adsorption mechanisms of Zn(II), Pb(II), and Fe(III) ions on the BLP/AgNPs composite could be due to physical adsorption and/or precipitation of metal ions. It is also suggested that the metal ions adsorption process may be due to chemisorption, electrostatic attraction between positively charged metal ions and nanosilver (Ag^o), and complex

Table 4. Adsorption kinetics models for the adsorption of Zn (II), Pb (II), and Fe (III) ions onto BLP/AgNPs.

Metal ion (adsorbate)	C_0 mg/l	$q_{e,exp}$ mg/g	Pseudo-first-order model			Pseudo -second-order model		
			$q_{e,cal}$ mg/g	K_1X10^{-3} min^{-1}	R^2	$q_{e,\ cal}$ mg/g	K_2X10^{-3} min^{-1}	R^2
Zn(II)	50	42	30.3	6.9	0.98	45.2	2.2	0.999
	100	79	61.2	6.21	0.99	86.4	0.91	0.999
	150	106	66.9	4.4	0.95	112	1	0.999
	200	129	84.6	4	0.95	138	0.81	0.999
	250	150	104	3	0.93	158	0.73	0.998
Pb(II)	50	45	35.3	3.8	0.97	50.2	1.4	0.999
	100	88	54.9	5.2	0.96	94.4	1.2	0.999
	150	131	82.3	5.1	0.95	136.7	0.79	0.997
	200	165	107	6.8	0.98	173.3	0.75	0.998
	250	184	114	3.9	0.95	191.6	0.82	0.999
Fe(III)	50	47	31.7	6.7	0.95	49.6	2.5	0.999
	100	91	63.5	6.7	0.98	96.7	1.1	0.999
	150	133	80.7	6.5	0.977	135.8	1.06	0.999
	200	166	98.8	5.2	0.95	171.5	0.94	0.999
	250	190	113	6.4	0.98	197.6	0.9	0.999

Table 5. Intraparticle diffusion model for Zn(II), Pb(II), and Fe(III) ions adsorption onto BLP/AgNPs.

Metal ion	C_o mg/l	Intraparticle diffusion model			
		K_{p1} mg/g $min^{0.5}$	R^2	K_{p2} mg/g $min^{0.5}$	R^2
Zn(II)	50	3	0.98	0.62	0.97
	100	4.8	0.99	1.6	0.98
	150	5.5	0.98	2.1	0.94
	200	6.1	0.99	2.3	0.94
	250	6.8	0.98	2.9	0.97
Pb(II)	50	6.6	0.99	1.5	0.98
	100	9.7	0.99	3.3	0.95
	150	11.9	0.99	3.7	0.98
	200	12.3	0.99	4.3	0.94
	250	15.3	0.98	6.3	0.97
Fe(III)	50	6.6	0.99	1.4	0.98
	100	9.7	0.99	3.3	0.95
	150	11.9	0.99	3.7	0.98
	200	12.3	0.99	4.3	0.94
	250	15.3	0.98	6	0.97

formation of reduced metal ions. Reduction and complexation may occur according to Eqs. (14) and (15),

$$Ag^{o}_{m} + (m/2)\ Zn^{2+} \longrightarrow mAg^{+} + (m/2)\ Zn^{o} \quad (14)$$

$$Ag^{o}_{n} + Zn^{2+} \longrightarrow Ag^{o}_{(n-2)}\ Zn^{o} + 2Ag^{+} \quad (15)$$

The functional groups on (BLP) surfaces may contribute to the adsorption of Zn(II), Pb(II), and Fe(III) ions as metal–H ion exchange or metal ion surface complexation adsorption or both. The adsorption of heavy metal ions may occur according to Eq. (16),

$$BLP/AgNPs + Fe^{3+}(aq) \rightarrow Fe^{3+}\text{-}BLP/AgNPs \quad (16)$$

The experimental study confirmed that the adsorption of heavy metal ions is reduced in an acidic medium and enhanced by increasing pH.

4. Conclusion

The present study focused on the fabrication of a cost-effective, new adsorbent. On banana leaves powder (BLP), silver nanoparticles (AgNPs) were synthesized and supported. The formation of (AgNPs) was confirmed spectrophotometrically at λ_{max} = 420 nm, impregnation of (AgNPs) with (BLP) was confirmed by the scanning electron microscopy, X-ray diffraction (XRD) patterns, and Fourier transform infrared spectroscopy analysis. The produced adsorbents (BLP/AgNPs) tested for Zn (II), Pb (II), and Fe (III) ions adsorption from aqueous solutions, The experimental findings revealed that the adsorption capacities of the adsorbent and sensitivity to Zn (II), Pb (II), and Fe (III) ions were greatly affected by the conditions of the adsorption process, the adsorption increased with increasing contact time, the dose of adsorbents, agitation speed, and temperature. It was also enhanced at low initial adsorbate concentrations but only slightly at high concentrations. The metal ions uptake was pH-controlled and the maximum sorption uptake was achieved at an optimum pH = 5 for Zn (II) ion, pH = 6 for Pb (II) and Fe (III) ions. The Zn (II), Pb (II), and Fe (III) ions uptake followed pseudosecond-order kinetics together with the intraparticle diffusion model. The adsorption processes were best fitted with Langmuir model, the removal of Zn (II), Pb (II), and Fe (III) ions by BLP/AgNPs were spontaneous and endothermic. The great adsorption capacity of BLP/AgNPs qualifies their use with effluents from a wide variety of industries.

Declarations

Author contribution statement

Mona A. Darweesh, Mohamed I. Ayad, Abdel Monem M. Ahmed: Conceived and designed the experiments; Analyzed and interpreted the data; Wrote the paper.

Mahmoud Y. Elgendy, W. A. Hammad: Conceived and designed the experiments; Performed the experiments; Analyzed and interpreted the data; Contributed reagents, materials, analysis tools or data; Wrote the paper.

N. M. Kamel Elsayed: Performed the experiments; Analyzed and interpreted the data; Contributed reagents, materials, analysis tools or data; Wrote the paper.

Funding statement

This research did not receive any specific grant from funding agencies in the public, commercial, or not-for-profit sectors.

Data availability statement

Data will be made available on request.

Declaration of interests statement

The authors declare no conflict of interest.

Additional information

No additional information is available for this paper.

References

[1] S.K. Pradhan, J. Panwar, S. Gupta, Enhanced heavy metal removal using silver-yttrium oxide nanocomposites as novel adsorbent system, J. Environ. Chem. Eng. 5 (6) (2017) 5801–5814. .

[2] K.O. Shittu, O. Ihebunna, Purification of simulated waste water using green synthesized silver nanoparticles of Piliostigma thonningii aqueous leave extract, Adv. Nat. Sci. Nanosci. Nanotechnol. 8 (4) (2017), 045003.

[3] R.S. Dubey, R. Xavier, Study on removal of toxic metals using various adsorbents from aqueous environment: a review, Sci. J. Eng. 1 (1) (2015) 30–36.

[4] F. Ge, M.M. Li, H. Ye, B.X. Zhao, Effective removal of heavy metal ions Cd^{2+}, Zn^{2+}, Pb^{2+}, Cu^{2+} from aqueous solution by polymer-modified magnetic nanoparticles, J. Hazard Mater. 211 (2012) 366–372.

[5] X. Wang, Y. Guo, L. Yang, M. Han, J. Zhao, X. Cheng, Nanomaterials as sorbents to remove heavy metal ions in wastewater treatment, J. Environ. Anal. Toxicol. 2 (7) (2012) 154.

[6] S. Afroze, T.K. Sen, A review on heavy metal ions and dye adsorption from water by agricultural solid waste adsorbents. Water, Air, Soil Pollut. 229 (7) (2018) 1–50.

[7] A. Ali, A. Mannan, I. Hussain, I. Hussain, M. Zia, Effective removal of metal ions from aquous solution by silver and zinc nanoparticles functionalized cellulose: isotherm, kinetics and statistical supposition of process, Environ. Nanotechnol. Monit. Manag. 9 (2018) 1–11.

[8] A.G.B. Pereira, A.F. Martins, A.T. Paulino, A.R. Fajardo, M.R. Guilherme, M.G.I. Faria, E.C. Muniz, Recent advances in designing hydrogels from chitin and chitin-Derivatives and their impact on environment and agriculture: a, Rev. Virtual Quim 9 (2017).

[9] I. Ali, V.K. Gupta, Advances in water treatment by adsorption technology, Nat. Prot. 1 (6) (2006) 2661–2667.

[10] G. Chauhan, P.U.K. Chauhan, Risk assessment of heavy metal toxicity through contaminated vegetables from waste, Int. J. Adv. Technol. Eng. Sci. 51 (2014) 444–460.

[11] O. Hakami, Y. Zhang, C.J. Banks, Thiol-functionalised mesoporous silica-coated magnetite nanoparticles for high efficiency removal and recovery of Hg from water, Water Res. 46 (12) (2012) 3913–3922.

[12] M.K. Uddin, A review on the adsorption of heavy metals by clay minerals with special focus on the past decade, Chem. Eng. J. 308 (2017) 438–462.

[13] A. Gupta, S.R. Vidyarthi, N. Sankararamakrishnan, Enhanced sorption of mercury from compact fluorescent bulbs and contaminated water streams using functionalized multiwalled carbon nanotubes, J. Hazard Mater. 274 (2014) 132–144.

[14] V.K. Gupta, A. Nayak, S. Agarwal, Bioadsorbents for remediation of heavy metals: current status and their future prospects, Environ. Eng. Res. 20 (1) (2015) 1–18.

[15] fao, Banana Market Review and Banana Statistics 2012–2013. Market and Policy Analyses of Raw Materials, Horticulture and Tropical (RAMHOT) Products Team. Rome, 2014.

[16] K.M. Al-Qahtani, Cadmium removal from aqueous solution by green synthesis zero valent silver nanoparticles with Benjamina leaves extract, Egypt. J. Aqua. Res. 43 (2017) 269–274.

[17] Y. Zhang, B. Wu, H. Xu, H. Liu, M. Wang, Y. He, B. Pan, Nanomaterials-enabled water and wastewater treatment, NanoImpact 3 (2016) 22–39. .

[18] S.T. El-Wakeel, R.S. El-Tawil, H.A. Abuzeid, A.E. Abdel-Ghany, A.M. Hashem, Synthesis and structural properties of MnO_2 as adsorbent for the removal of lead (Pb^{2+}) from aqueous solution, J. Taiwan Inst. Chem. Eng. 72 (2017) 95–103.

[19] S.G. Kim, N. Hagura, F. Iskandar, K. Okuyama, Characterization of silica-coated Ag nanoparticles synthesized using a water-soluble nanoparticle micelle, Adv. Powder Technol. 20 (2009) 94–100.

[20] E. Vélez, G.E. Campillo, G. Morales, C. Hincapié, J. Osorio, O. Arnache, F. Jaramillo, Mercury removal in wastewater by iron oxide nanoparticles, J. Phys. C 687 (1) (2016), 012050.

[21] R.S. El-Tawil, S.T. El-Wakeel, A.E. Abdel-Ghany, H.A. Abuzeid, K.A. Selim, A.M. Hashem, Silver/quartz nanocomposite as an adsorbent for removal of mercury (II) ions from aqueous solutions, Heliyon 5 (9) (2019), e02415.

[22] M.A. Salem, R.G. Elsharkawy, M.I. Ayad, M.Y. Elgendy, Silver nanoparticles deposition on silica, magnetite, and alumina surfaces for effective removal of Allura red from aqueous solutions, J. Sol. Gel Sci. Technol. 91 (3) (2019) 523–538.

[23] T.H. Liou, Development of mesoporous structure and high adsorption capacity of biomass-based activated carbon by phosphoric acid and zinc chloride activation, Chem. Eng. J. 158 (2) (2010) 129–142.

[24] P. Barpanda, G. Fanchini, G.G. Amatucci, Structure, surface morphology and electrochemical properties of brominated activated carbons, Carbon 49 (7) (2011) 2538–2548. .

[25] C. Ashish, K. Balbir, XRD and physicochemical evaluation of Hibiscus sabdariffa cellulose-butyl acrylate-co-vinyl monomer graft, Am. J. Biochem. Mol. Bio. 3 (1) (2013) 61–70. .

[26] B.S. Kaith, A.S. Singha, S.K. Sharma, Synthesis of graft copolymers of binary vinyl monomer mixtures and flax fiber using FAS-KPS redox system, Int. J. Chem. Sci. 2 (2004) 37–43. .

[27] X. Du, J. He, J. Zhu, L. Sun, S. An, Ag-deposited silica-coated Fe_3O_4 magnetic nanoparticles catalyzed reduction of p-nitrophenol, Appl. Surf. Sci. 258 (2012) 2717–2723.

[28] Q. Chen, J. Zheng, L. Wen, C. Yang, L. Zhang, A multi-functional-group modified cellulose for enhanced heavy metal cadmium adsorption: performance and quantum chemical mechanism, Chemosphere 224 (2019) 509–518.

[29] C.M. Popescu, G. Singurel, M.C. Popescu, C. Vasile, D.S. Argyropoulos, S. Willför, Vibrational spectroscopy and X-ray diffraction methods to establish the differences between hardwood and softwood, Carbohydr. Polym. 77 (4) (2009) 851–857. .

[30] L.C. Over, M.A. Meier, Sustainable allylation of organosolv lignin with diallyl carbonate and detailed structural characterization of modified lignin, Green Chem. 18 (1) (2016) 197–207.

31]] D. Dos Santos Dias, F.A. Faria, L. Mattiolli, M.V. Capela, J.M.V. Capela, M.S. Crespi, C.A. Ribeiro, Moisture sorption of biochar from banana pseudostem fibers according to the pyrolysis temperature, J. Therm. Anal. Calorim. 138 (5) (2019) 3825–3832.

[32] W. Li, Y. Zhu, Structural characteristics of coal vitrinite during pyrolysis, Energy Fuels 28 (6) (2014) 3645–3654.

[33] P.K. Adapa, C. Karunakaran, L.G. Tabil, G.J. Schoenau, Potential applications of infrared and Raman spectromicroscopy for agricultural biomass, Agric. Eng. Int.: CIGR J. (2009).

[34] R. Xiao, S. Wang, R. Li, J.J. Wang, Z. Zhang, Soil heavy metal contamination and health risks associated with artisanal gold mining in Tongguan, Shaanxi, China, Ecotoxicol. Environ. Saf. 141 (2017) 17–24.

[35] C.H. Chia, B. Gong, S.D. Joseph, C.E. Marjo, P. Munroe, A.M. Rich, Imaging of mineral-enriched biochar by FTIR, Raman and SEM–EDX, Vib. Spectrosc. 62 (2012) 248–257.

[36] M.R. Awual, M. Ismael, M.A. Khaleque, T. Yaita, Ultra-trace copper (II) detection and removal from wastewater using novel meso-adsorbent, J. Ind. Eng. Chem. 20 (4) (2014) 2332–2340.

[37] T. Murugan, A. Ganapathi, R. Valliappan, Removal of dyes from aqueous solution by adsorption on biomass of mango (Mangifera indica) leaves, E-j. Chem. 7 (3) (2010) 669–676.

38]] D. Kaliannan, S. Palaninaicker, P. Velayutham, V. Palanivel, A.J. Kumar, Novel synthesis of Chrysanthemum indicum flower as an adsorbent for the removal of direct Congo red from aqueous solution, Desalination Water Treat. 113 (2018) 270–280. .

[39] N.H. Abdullah, K. Shameli, E.C. Abdullah, L.C. Abdullah, Solid matrices for fabrication of magnetic iron oxide nanocomposites: synthesis, properties, and application for the adsorption of heavy metal ions and dyes, Compos. B Eng. 162 (2019) 538–568.

[40] H. Ding, X. Luo, X. Zhang, H. Yang, Alginate-immobilized Aspergillus Niger: characterization and biosorption removal of thorium ions from radioactive wastewater, Colloids Surf. A Physicochem. Eng. Asp. 562 (2019) 186–195.

[41] M. Waseem, S.T. Muntha, M. Nawaz, W. Rehman, M.A. Rehman, K.H. Shah, Effect of heat treatment on the efficient adsorption of Cd^{2+} ions by nanosized SiO_2, TiO_2 and their composite, Mater. Res. Express 4 (1) (2017), 015017. .

[42] R. Bhaumik, N.K. Mondal, Optimizing adsorption of fluoride from water by modified banana peel dust using response surface modelling approach, Appl. Water Sci. 6 (2) (2016) 115–135. .

[43] R. Gong, Y. Ding, H. Liu, Q. Chen, Z. Liu, Lead biosorption and desorption by intact and pretreated Spirulina maxima biomass, Chemosphere 58 (1) (2005) 125–130. .

[44] Z. Elouear, R.B. Amor, J. Bouzid, N. Boujelben, Use of phosphate rock for the removal of Ni^{2+} from aqueous solutions: kinetic and thermodynamics studies, J. Environ. Eng. 135 (4) (2009) 259–265.

[45] A. Saeed, M. Iqbal, M.W. Akhtar, Removal and recovery of lead (II) from single and multimetal (Cd, Cu, Ni, Zn) solutions by crop milling waste (black gram husk), J. Hazard Mater. 117 (1) (2005) 65–73.

[46] X. Wang, X. Liang, Y. Wang, X. Wang, M. Liu, D. Yin, Y. Zhang, Adsorption of Copper (II) onto activated carbons from sewage sludge by microwave-induced phosphoric acid and zinc chloride activation, Desalination 278 (1-3) (2011) 231–237. .

[47] E.M. Soliman, S.A. Ahmed, A.A. Fadl, Reactivity of sugar cane bagasse as a natural solid phase extractor for selective removal of Fe (III) and heavy-metal ions from natural water samples, Arab. J. Chem. 4 (1) (2011) 63–70. .

[48] D. Kaliannan, S. Palaninaicker, V. Palanivel, M.A. Mahadeo, B.N. Ravindra, S. Jae-Jin, A novel approach to preparation of nano-adsorbent from agricultural wastes (Saccharum officinarum leaves) and its environmental application, Environ. Sci. Pollut. Res. 26 (6) (2019) 5305–5314.

[49] M.A. Darweesh, M.Y. Elgendy, M.I. Ayad, A.M. Ahmed, N.K. Elsayed, W.A. Hammad, Adsorption isotherm, kinetic, and optimization studies for copper (II) removal from aqueous solutions by banana leaves and derived activated carbon, S. Afr. J. Chem. Eng. 40 (2022) 10–20.

[50] B. Abbar, A. Alem, S. Marcotte, A. Pantet, N.D. Ahfir, L. Bizet, D. Duriatti, Experimental investigation on removal of heavy metals (Cu^{2+}, Pb^{2+}, and Zn^{2+}) from aqueous solution by flax fibres, Process Saf. Environ. Protect. 109 (2017) 639–647.

[51] S. Mustapha, D.T. Shuaib, M.M. Ndamitso, M.B. Etsuyankpa, A. Sumaila, U.M. Mohammed, M.B. Nasirudeen, Adsorption isotherm, kinetic and thermodynamic studies for the removal of Pb (II), Cd (II), Zn (II) and Cu (II) ions from aqueous solutions using Albizia lebbeck pods, Appl. Water Sci. 9 (6) (2019) 1–11. .

[52] P. Maneechakr, S. Karnjanakom, Environmental surface chemistries and adsorption behaviors of metal cations (Fe^{3+}, Fe^{2+}, Ca^{2+} and Zn^{2+}) on manganese dioxide-modified green biochar, RSC Adv. 9 (42) (2019) 24074–24086.
[53] S. Chakravarty, A. Mohanty, T.N. Sudha, A.K. Upadhyay, J. Konar, J.K. Sircar, K.K. Gupta, Removal of Pb (II) ions from aqueous solution by adsorption using bael leaves (Aegle marmelos), J. Hazard Mater. 173 (1-3) (2010) 502–509.
[54] A. Üçer, A. Uyanik, Ş.F. Aygün, Adsorption of Cu (II), Cd (II), Zn (II), Mn (II) and Fe (III) ions by tannic acid immobilised activated carbon, Sep. Purif. Technol. 47 (3) (2006) 113–118. .
[55] M.R. Karim, M.O. Aijaz, N.H. Alharth, H.F. Alharbi, F.S. Al-Mubaddel, M.R. Awual, Composite nanofibers membranes of poly (vinyl alcohol)/chitosan for selective lead (II) and cadmium (II) ions removal from wastewater, Ecotox. Environ. Safety 169 (2019) 479–486. .
[56] Y. Kismir, A.Z. Aroguz, Adsorption characteristics of the hazardous dye Brilliant Green on Saklıkent mud, Chem. Eng. J. 172 (1) (2011) 199–206.
[57] A.M. Ahmed, M.I. Ayad, M.A. Eledkawy, M.A. Darweesh, E.M. Elmelegy, Removal of iron, zinc, and nickel-ions using nano bentonite and its applications on power station wastewater, Heliyon 7 (2) (2021), e06315.
58]] K. Kaya, E. Pehlivan, C. Schmidt, M. Bahadir, Use of modified wheat bran for the removal of chromium (VI) from aqueous solutions, Food Chem. 158 (2014) 112–117. .
[59] N.E. Belkhouche, N. Benyahia, Modeling of adsorption of Bi (III) from nitrate medium by impregnated resin D2EHPA/XAD-1180, J. Surf. Eng. Mater. Adv. Technol. 1 (2) (2011) 30–34.
[60] A.M. El-Sawy, H.A. Moa'mena, M.A. Darweesh, N.A. Salahuddin, Synthesis of modified PANI/CQDs nanocomposite by dimethylgyloxime for removal of Ni (II) from aqueous solution, Surface. Interface 26 (2021) 101392.